Computational fluid dynamics analysis of the fluid environment of 3D printed gradient structure in interfacial tissue engineering

Bin Zhang

Department of Mechanical and Aerospace, Brunel University London, London, United Kingdom

ABSTRACT

Mass transport properties within three-dimensional (3D) scaffold are essential for tissue regeneration, such as various fluid environmental cues influence mesenchymal stem cells differentiation. Recently, 3D printing has been emerging as a new technology for scaffold fabrication by controlling the scaffold pore geometry to affect cell growth environment. In this study, the flow field within scaffolds in a perfusion system was investigated with uniform structures, single gradient structures and complex gradient structures using computational fluid dynamics (CFD) method. The CFD results from those uniform structures indicate the fluid velocity and fluid shear stress within the scaffold structure increased as the filament diameter increasing, pore width decreasing, pore shape decreased from 90° to 15°, and layer configuration changing from lattice to stagger structure. By assembling those uniform structure as single gradient structures, it is noted that the fluid dynamic characterisation within the scaffold remains the same as the corresponding uniform structures. A complex gradient structure was designed to mimic natural osteochondral tissue by assembly the uniform structures of filament diameter, pore width, pore shape and layer configuration. The results show that the fluid velocity and fluid shear stress within the complex gradient structure distribute gradually increasing and their maximum magnitude were from 1.15 to 3.20 mm/s, and from 12 to 39 mPa, respectively. CFD technique allows the prediction of velocity and fluid shear stress within the designed 3D gradient scaffolds, which would be beneficial for the tissue scaffold development for interfacial tissue engineering in the future.

Introduction

Tissue engineering aims to fabricate biological tissue scaffolds with the goal of repairing or regenerating the functions of diseased or damaged natural tissue [1–3]. Design and production of tissue scaffolds that mimic the complex structural and functional features of natural tissues are the most key issues of tissue engineering strategy [4]. Although natural tissues have their own complex structure, an even more complex case in terms of developing tissue scaffold would encounter at the interfacial tissues, where two distinct tissues come together [4,5]. For example, osteochondral tissue is one of the common interfacial tissues that compose of cartilage and bone, which is especially susceptible to injury and tear when high strain fields are present [6]. Engineering osteochondral tissue still remains a challenge due to their complexities such as cell type, structure and microfluid environment.

The osteochondral tissue exhibits a transition from soft cartilage, calcified cartilage to the subchondral bone; this transition exhibits gradient characteristics. Cartilage is a highly interconnected tissue with a porosity of 60–85 %; while the subchondral bone contains cortical bone and trabecular bone. The pore width varies from 0.1 to 2000 μm and the porosity changes from 5 to 90 % from the top to the bottom of the subchondral bone. Calcified cartilage is in the transition zone from cartilage and subchondral bone. Chondrocyte is existed in both of cartilage and calcified tissue while, osteoblasts is in the bone tissue. Mesenchymal stem cells (MSCs) are multi-potential stromal cells that existed in osteochondral tissue, which are able to differentiate into many cell types such as osteoblasts and chondrocytes.

The osteochondral tissue scaffolds described in many research studies exhibit a gradient property to mimic osteochondral tissue attributes [7–10]. Tissue scaffolds should have a porous structure to allow the flow of culture medium with cells, nutrients, and oxygen within the scaffold. The appropriate mechanical stimulus should be able to be transmitted to the scaffold so that cells can follow specific differentiation pathways [11]. Fluid flow can be applied to scaffolds and transmit mechanical stimulus to cells attached to the scaffold surface, which stimulates tissue differentiation by fluid shear stress [12]. Kim, et al. [13] applied a shear flow to MSCs cultured in perfusion bioreactor with

Table 1

The osteochondral tissue porosity and fluid shear stress threshold of cell proliferation and differentiation [3,14, 16-18].

	Porosity	Main cell type	Fluid shear stress threshold (mPa)	MSCs differentiation (mPa)
Cartilage	60–85 %	Chondrocyte & MSCs	150–200	20–100
Calcified cartilage	Porosity gradually vary (>50 %)	Chondrocyte &osteoblast & MSCs	Transition zone from cartilage and bone	
Bone	5–90 %	Osteoblast & MSCs	80–300	12 −30

the flow shear stress in the range of 0.012 to 0.015 Pa. They found that fluid shear stress significantly induced alkaline phosphatase activity and the expression of osteogenic differentiation, *i.e.*, Runx2. Lee, et al. [14] mentioned that the exposure to low magnitudes of shear stress (0.03 Pa) induced osteogenic differentiation, including increased expression of osteopenia and osteocalcin. Kim, et al. [15] showed that the human MSCs in perfusion fluid flow may experience shear stress in the range of 0.01 to 0.1 Pa. Those studies demonstrated that MSCs can differentiate into the bone cell and cartilage cells under the stimulation of fluid shear stress. Although the feasible shear stress for MSCs to express the osteogenic differentiation is relatively different from study to study, they demonstrated that the differentiation of bone tissue should be in a low shear stress environment *in vitro* – in the range of 12 mPa to 30 mPa; while the differentiation of cartilage tissue should be in a high shear
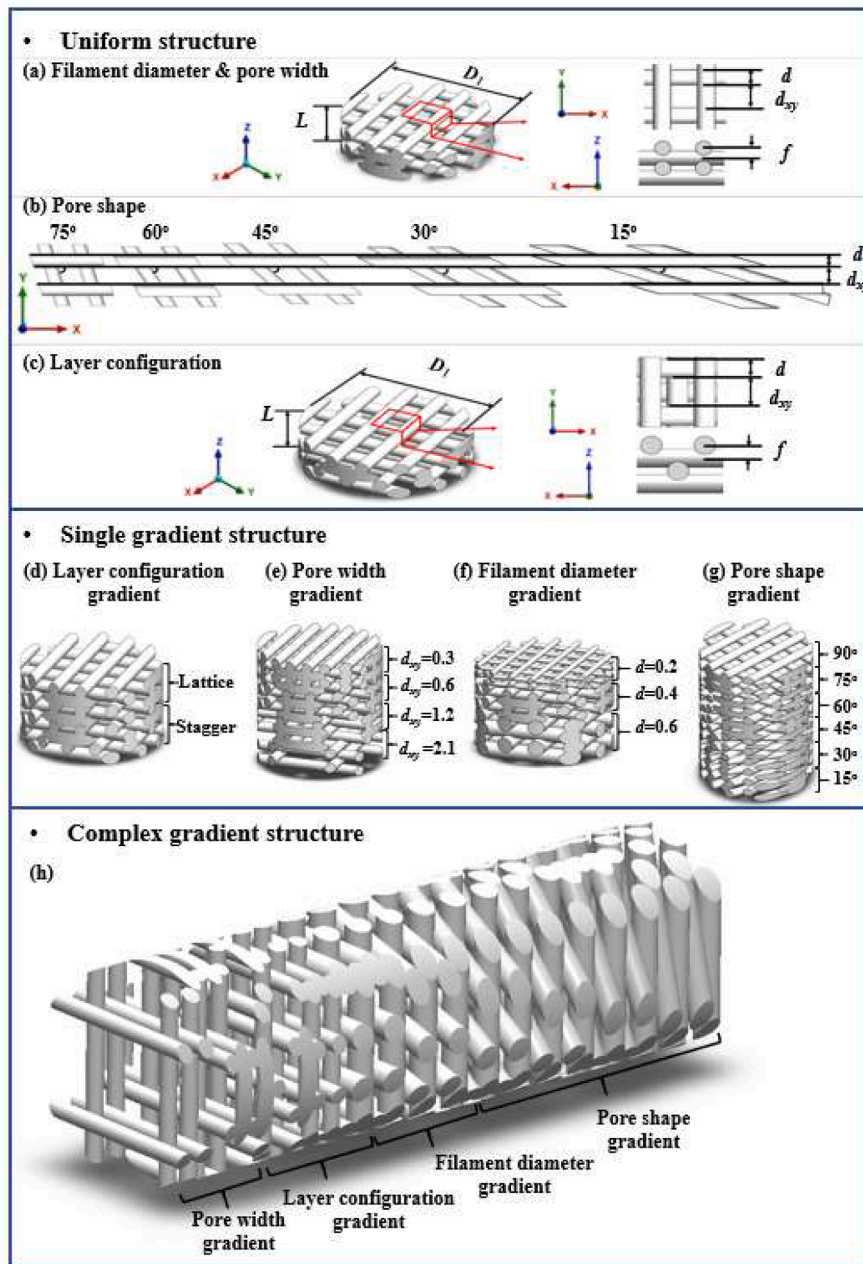
Fig. 1. CAD models of uniform structure with the variable filament diameter and pore width (a), pore shape (b) and layer configuration (c). Single gradient structure with the layer configuration gradient (d), pore width gradient (e) with the pore width (d_{xy}) changes from 0.3 to 2.1 mm, filament diameter gradient (f) with the filament diameter (*d*) change from 0.2 to 0.6 mm, pore shape gradient (g) with the filament intersection angles changes from 90° to 15° Complex gradient structure with a combination gradient of layer configuration, pore width, filament diameter and pore shape (h).
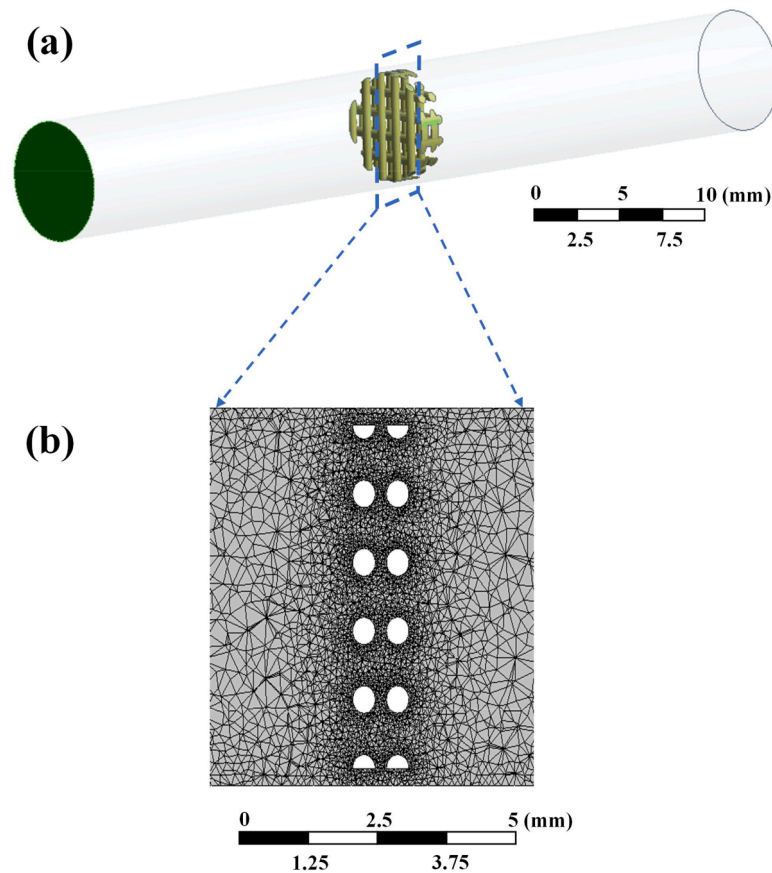
Fig. 2. The setup (a) and mesh (b) of CFD simulations. The mesh is demonstrated in a cross-section cutting through the scaffold.

stress environment *in vitro* – in the range of 20 mPa to 100 mPa. As summarised in Table 1, there existed shear stress boundaries are crossed, cell-driven biochemical reactions are initiated, which affect cell differentiate into various tissue from one type to another. There is a balance between fluid shear stress and fluid velocity. A higher fluid velocity could help cell metabolism; however, it would generate a relatively higher fluid shear stress. The shear stress is better not higher than the tolerated threshold of the cell.

Although the above studies showed that the feasible fluid shear stress facilitated MSCs differentiation, they did not investigate the distribution of fluid shear stress at each specific location of the scaffold under specific fluid flows. Notably, it is vital to develop scaffolds for the repairing of interfacial tissue, such as osteochondral tissue that has cartilage phase and bone phase. By accurately controlling the distribution of fluid shear stress on the scaffold could directionally induce cells to differentiate to various cells, *i.e.*, bone or cartilage.

Recently, due to the 3D printing emerging, it creates a possibility to control the microstructure of scaffold with predesigned computational added design (CAD) structures [3,19-22]. Some studies investigating the influence of scaffold pore distribution and pore geometries on fluid shear stress [23–25]. Boschetti, et al. [23] showed that the pore width is a variable strongly influencing the predicted the level of shear stress, whereas the porosity is a variable strongly affecting the statistical distribution of the shear stresses, but not their magnitude. Melchels, et al. [24] simulated the fluid shear stress using computational fluid dynamic (CFD) modelling within uniform gyroid scaffold in perfusion fluid and compared the simulation results with *in vitro* experiments. The *in vitro* experimental results revealed that there was the highest cell density in the region of the scaffold where the wall shear stress of the fluid flow was the highest (3.8 mPa).

Based on the above studies, the distribution of fluid field within

scaffold can affect the cell distribution, and MSCs show the potential to differentiate various cells with influencing by fluid shear stress. However, it is difficult to detect the shear stress distribution within the scaffold during *in vitro* or *in vivo* experiments [26,27]. Computational modelling can be used together with experimental data to investigate the effects of fluid shear stress on cell differentiation [28–33]. This study aims to use CFD modelling to analyse the influence of scaffold with variable pore geometries on the response of the interstitial fluid velocity and surface shear stress within the scaffold pores at the initial stage of a perfusion bioreactor cell culture. It is hypothesised that various scaffold pore geometries create areas with different fluid flow distribution and further affect the mechanical stimulus on MSCs differentiation. Uniform structure with the variable filament diameter, pore width, pore shape and layer configuration were proposed, and their fluid dynamic characterisations were investigated. Single gradient and complex gradient were assembled by those uniform structures so that to create gradient fluid dynamic environment. To the best of our knowledge, although change the stack position of the filament is a common 3D printing method for scaffold fabrication, there is no study has been systematically done to investigate the fluid flow inside 3D printed scaffolds with different pore geometries.

Methodology

Design of scaffold geometry

To mimic the fluid environment in a perfusion bioreactor, three categories of CAD scaffolds with designed as layered cylinders with a diameter of 5 mm using Solidworks software (Dassault Systèmes, Vélizy-Villacoublay, France). The three categories of CAD scaffolds are the uniform structure, single gradient structure, and complex gradient

structure, as shown in Fig. 1.

The uniform structure has the same architecture from the top to bottom, and there are three types. The first type is a lattice structure with variable filament diameter and pore width. Figure (a) shows the top and side views of the 90° lattice unit. The pore width (d_{xy}) is defined as the inter-filament spacing, which varies from 0.3 to 2.1 mm, and the filament diameter (d) varies from 0.2 to 0.6 mm. The setting parameters of filament diameter and pore width are in the range of osteochondral tissue scaffold from the literature [34–36]. The layer overlap (f) refers to the distance between the middle plane of two adjacent layers. Considering the practical condition of 3D printing, layer overlap (f) was fixed as the 0.7 times of filament width for all structures. The second type is a lattice structure with different pore shape. The pore shape was defined as the filament inter-section angles of 15°, 30°, 45°, 60°, 75° and 90°, respectively. Fig. 1(b) shows the unit structure of scaffold with variable pore shape and all structures have the same filament diameter (d) and pore width (d_{xy}). The third type of 3D constructs was a staggered structure designed by changing layer configuration and an offset building of the lattice structure, in Fig. 1(c). The filament width and pore width of the staggered structure were kept as the same as the lattice one. All uniform scaffold structures are formed with four layers, which is the minimum number of layers for the repetition of a cycle for stagger structure.

The single gradient structures have four types, as shown in Fig. 1 (d-g), which are layer configuration gradient, pore width gradient, filament diameter gradient and pore shape gradient. Layer configuration gradient is composed of lattice and stagger structures in Fig. 1(d). Pore width gradient is constituted by the uniform structures with variable pore width from 0.3 to 2.1 mm, as shown in Fig. 1(e). Similarly, the uniform structures with variable filament diameter from 0.2 to 0.6 mm are created the filament diameter gradient, in Fig. 1(f). While the pore shape gradient represents the combination of the lattice scaffold with the filament intersection angles changing from 90° to 15°, as shown in Fig. 1 (g). Complex gradient structure is the assembly of single gradient structures. The gradient assembly order is determined after the investigation of the influence of pore geometries on the fluid dynamic properties. Complex gradient structure is the combination of various pore width, layer configuration, filament diameter and pore shape, as shown in Fig. 1(h).

Porosity analysis

The solid volume (V_{solid}) of constructs from the CAD model was obtained using the "Tools>Evaluate>Mass property" function in Solidworks software. The porosity was calculated as from the percentage of the 3D construct solid volume (V_{solid}) to the total volume (V_{total}) of the scaffold using Equation (Eq) 1 and 2

$$V_{total} = \pi \left(\frac{D_1}{2} \right) L \tag{1}$$

$$Porosity = \left(1 - \frac{V_{Solid}}{V_{total}} \right) \tag{2}$$

Computational fluid dynamics simulation

The CAD scaffold models were imported into Fluent software (ANSYS, Inc., Canonsburg, Pennsylvania, USA) for computational fluid dynamics simulation (CFD) simulations. As shown in Fig. 2(a), the scaffold is placed in the middle of a 40 mm long tube. The diameter of the tube can completely enclose the cylindrical scaffold. The distance between the inlet and the scaffold is 20 mm, which is sufficiently long to create a fully developed laminar flow condition.

Fig. 2(b) shows the mesh of the fluid domain. The mesh is created with tetrahedral elements using 'curvature' setting in Fluent software; the curvature ratio is set as the default value 1.2. This meshing method

Table 2
A summary of element numbers and CFD computational time of five-element sizes for the pores of the 90° lattice scaffold.

Minimum element sizes(µm)	Numbers of tetrahedral elements	CFD computational time (min)	Maximum velocity (mm/s)	Maximum wall shear stress (mPa)
128	921,560	2	1.77	27.15
64	1,235,833	6.5	1.95	29.88
32	1,285,201	8	2.11	30.90
16	2,087,344	11	2.14	31.40
4	3,057,485	20	2.15	31.40

maintains relatively larger elements where possible whereas ensures refinement near irregular boundaries to reduce computational cost; therefore, it can provide a smooth transition from the surroundings of the scaffold to the internal pores. The minimum element size is 16 µm inside the pores and the maximum element size is 1 mm far away from the scaffold. The total number of tetrahedral elements is 24 million, which is determined by a mesh sensitivity study.

The incompressible Newtonian fluid and laminar flow condition are assumed. The viscosity and density of the fluid are 0.001 Pa·s and 1000 kg/m^3, respectively, which are similar to the cell culture medium at 37°C. The inlet velocity is applied using a 3D parabolic profile to ensure that a laminar flow could be fully developed before reaching the scaffold in the tube. The average inlet velocity is chosen as 0.5 mm/s to obtain physiological fluid shear stress on cells [37]. The outlet boundary condition is set as zero pressure, and non-slip wall condition is applied at scaffold surfaces and the tube.

### Results

Mesh sensitivity test for CFD modelling

A mesh sensitivity test is conducted to determine the appropriate mesh size for CFD simulations. The maximum flow velocity and fluid shear stress were compared between five gradually reducing mesh sizes (Table 2) for the uniform 90° lattice scaffold in CFD modelling. The maximum velocity only changes about 0.5 % by reducing the minimum element size from 16 µm to 4 µm; however, a minimum element size of 4 µm requires almost twice as much computational time as a minimum element size of 16 µm. There is no change of maximum shear stress when reducing the minimum element size from 16 µm to 4 µm. Therefore, a minimum element size of 16 µm is chosen for the pores in CFD modelling.

Uniform structure

The fluid dynamics inside pores of scaffolds are analysed from two aspects by CFD modelling: the fluid velocity and shear stress. Variable uniform scaffolds are modelled in a setup as shown in Fig. 2, including scaffolds with the variable filament diameter, pore width, pore shape and layer configuration. The fluid velocity and shear stress are compared at the same location between different scaffold structures.

Influence of filament diameter

Regarding lattice scaffolds with variable filament diameter (d) changing from 0.2 mm to 0.6 mm, a higher fluid velocity was observed in the middle of the pores of scaffolds. Fig. 3(a) shows the longitudinal plane view of fluid velocity within the lattice scaffold. The maximum fluid velocity magnitude of 1.7 mm/s was found in the lattice scaffold with the filament diameter of 0.2 mm. The fluid velocity in the middle of the pore increases with the filament diameter changing from 0.2 mm to 0.6 mm. The maximum fluid velocity magnitude of 2.2 mm/s and 2.7 mm/s for scaffold with the filament diameter of 0.4 mm and 0.6 mm, respectively.
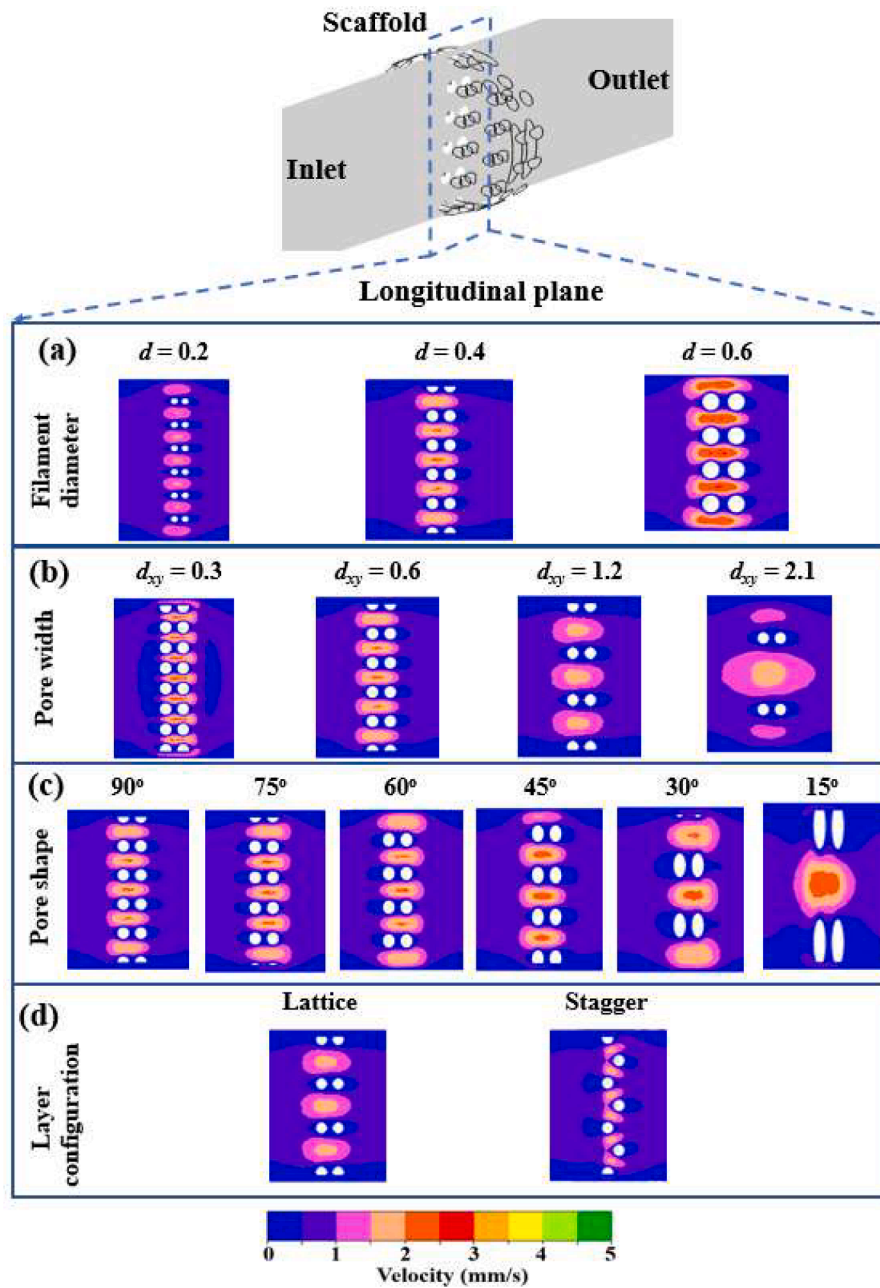
Fig. 3. Fluid velocity distribution within the uniform scaffold structure with variable filament diameter (a); pore width (b); pore shape (c); and layer configuration (d).

Meanwhile, fluid shear stress is directly proportional to the velocity gradient. The fluid shear stress distribution from the transverse plane in scaffolds is shown in Fig. 4(a). The fluid shear stress increased with the lattice scaffold filament diameter changing from 0.2 mm to 0.6 mm. The trend is similar to the fluid velocity, and the maximum fluid shear stress locates on the filament edge of unit pores. The maximum fluid shear stress on the scaffold with the filament diameter of 0.2 mm, 0.4 mm and 0.6 mm were 28 mPa, 33 mPa and 39 mPa, respectively.

Influence of pore width

For those lattice scaffolds with variable pore width (d_{xy}) changing from 0.3 mm to 2.1 mm, the higher fluid velocity was observed in the middle of the pores of the lattice scaffolds, as shown in Fig. 3(b). The fluid velocity in the middle of the pore decreases with the pore width changing from 0.3 mm to 2.1 mm. The maximum fluid velocity magnitude of 1.95 mm/s was found in the middle of lattice scaffold with

pore width of 2.1 mm; while for scaffold with pore width of 0.3 mm, the maximum fluid velocity magnitude was 2.9 mm/s.

Meanwhile, the fluid shear stress distribution in scaffolds on a transversal plane is shown in Fig. 4(b). The maximum fluid shear stress locates on the filament edge of unit pores. The fluid shear stress decreased with the lattice scaffold pore width changing from 0.3 mm to 2.1 mm. The maximum fluid shear stress on the scaffold with a pore width of 2.1 and 0.3 were 11.5 and 39.7 mPa, respectively.

Influence of pore shape

Fig. 3(c) shows the fluid velocity distributions within the scaffold with variable pore shape from the view of a transversal plane. The fluid velocity in the middle of the pore gradually increases with the filament intersection angle changing from 90° to 15°. The highest fluid velocity magnitude of 2.51 mm/s is found in the middle of 15° lattice scaffold, which is around seven times the inlet velocity (0.5 mm/s). While for 90°
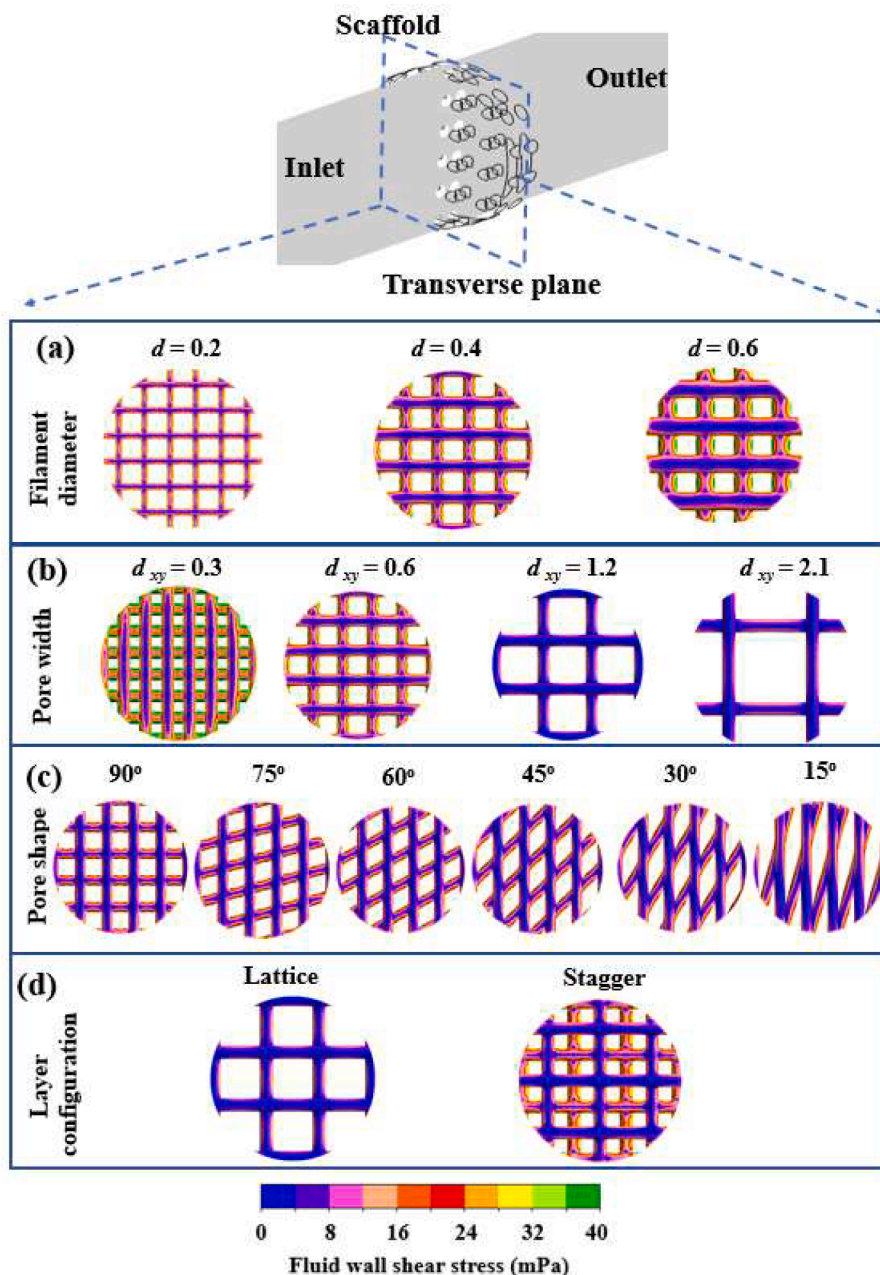
Fig. 4. Fluid shear stress distribution within the uniform scaffold structure with variable filament diameter (a); pore width (b); pore shape (c); and layer configuration (d).

lattice scaffold, the maximum fluid velocity is 2.1 mm/s. The gradual increase in maximum fluid velocity within the scaffold from 90 °C to 15 °C is potentially due to the difference in pore numbers. As shown in Fig. 4(c), the pore number for the 15 °C scaffold is 5, while it is 21 for the 90 °C scaffold. Although the 90 °C scaffold has more pores, the single pore size of the 15 °C scaffold is higher than that of the 90 °C scaffold. Consequently, this results in both the 15 °C and 90 °C scaffolds having the same porosity, as mentioned in section 3.3.3.

The fluid shear stress distribution within scaffolds is shown in Fig. 4 (c). The fluid shear stress slightly increased with the lattice scaffold angles decreasing from 90° to 15°, which are 19 mPa and 23 mPa, respectively. It is noticed that although there is *circa* 20% difference of fluid shear stress that caused by pore shape-changing (from 90° to 15°), the influence of pore width would give a much greater effect on fluid velocity and shear stress than pore shape and filament diameter.

Influence of layer configuration

Fig. 3(d) shows the fluid velocity distribution within stagger scaffolds which is offset structure based on the lattice scaffold. It is noticed that the fluid distributaries two separate branch due to the offset layer and the higher fluid velocity was also observed in the middle of the pores. The maximum fluid velocity magnitude of 1.9 mm/s was found in the middle of stagger scaffold; while for lattice scaffold, the maximum fluid velocity magnitude was 1.7 mm/s.

The fluid shear stress distribution in scaffolds is shown in Fig. 4(d). The fluid shear stress within the lattice scaffold was 12.5 mPa; while the fluid shear stress with the stagger scaffold was higher than lattice structure, which is 31.1 mPa. This possibly because that fluid was separate as two branches and spatially decrease the pore volume, and the offset layer hind the fluid flow, thus creating the relatively higher shear stress on the offset layer.
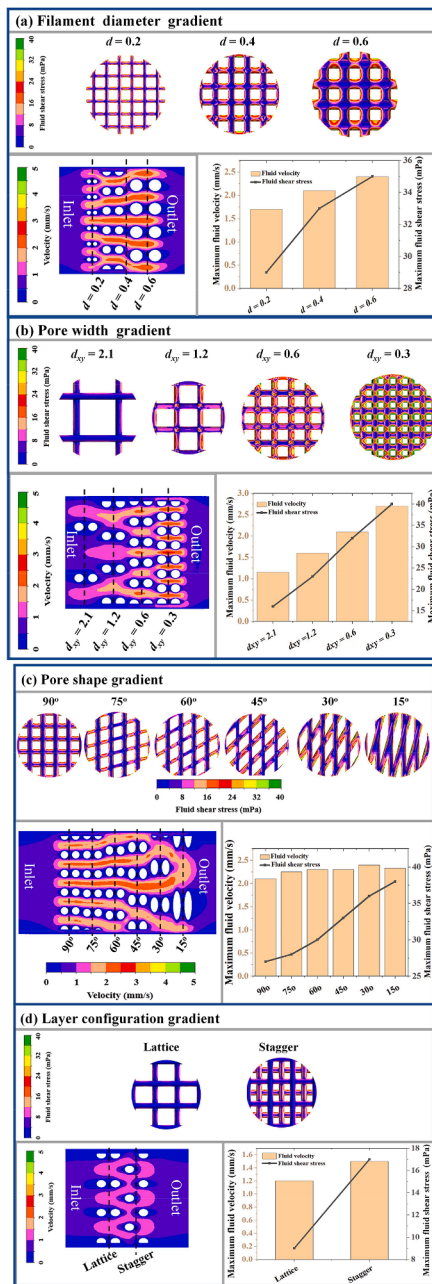
Fig. 5. The distribution and magnitude of fluid velocity and shear stress within the single gradient structure with filament diameter gradient (a); pore width gradient (b); pore shape gradient (c); and layer configuration gradient (d).

Single gradient structure

As mentioned earlier, the gradient scaffold structure aims to mimic the natural interfacial tissue, creating a gradient microenvironment that simulates the generated shear stress within the 3D scaffold. This is done to achieve the idea of manipulating scaffold geometry to control cell differentiation, specifically in the context of bone and cartilage [25,30]. The study proposes the concept of assembling variable geometries to create a gradient structure. This includes a filament diameter gradient, pore width gradient, pore shape gradient, and layer configuration gradient.

The influence of filament diameter gradient

In Fig. 5(a), regarding the filament diameter gradient that with filament diameter (d) changing from 0.2 to 0.6 mm, their maximum fluid velocity magnitude increased. The fluid velocity magnitude of the scaffold with the filament diameter of 0.2 mm is 1.4 times higher than that with the filament diameter of 0.6 mm. This possible due to that although those scaffolds have the same pore width, the scaffold with larger filament diameter could create greater hinder to the fluid flow comparing with the scaffold with smaller filament diameter.

Meanwhile, the fluid shear stress increased with the lattice scaffold filament diameter changing from 0.2 mm, 0.4 mm to 0.6 mm. The maximum fluid shear stress magnitude of the scaffold with the filament diameter of 0.6 mm was 1.21 times higher than the one with the filament diameter of 0.2 mm. It is noted that the trend of the maximum magnitude of wall shear stress within the filament gradient structure is kept as the same as the corresponding of their uniform structures. Thus, by the assembly of the scaffold with filament diameter from 0.2 to 0.6 mm within a single filament gradient scaffold structure could create a gradient increasing change of fluid velocity and fluid shear stress.

The influence of pore width gradient

The pore width gradient that with pore width (d_{xy}) changing from 2.1 to 0.3 mm, their maximum fluid velocity magnitude increased. In Fig. 5(b), the fluid velocity magnitude of the scaffold with the pore width of 0.3 mm is 2.35 times higher than that with the pore width of 2.1 mm. This could be due to that larger pore give relatively wider space for fluid flow through than smaller pore so that generate less velocity. Similar results also can be found in other studies [38–40].

Meanwhile, the fluid shear stress increased with the lattice scaffold pore width decreasing from 2.1 to 0.3 mm within the single pore width gradient structure. This trend kept the same as their corresponding uniform structures. The maximum fluid shear stress magnitude of the scaffold with the filament diameter of 0.6 mm was 2.5 times higher than the one with the filament diameter of 0.2 mm. By assembly of the scaffold with pore width from 0.3 to 2.1 mm within a single filament gradient scaffold structure could create a gradient change of fluid velocity and fluid shear stress.

The influence of pore shape gradient

In Fig. 5(c), the single pore shape gradient that with filament intersection angle changing from 90° to 15°, and their maximum fluid velocity magnitude had a slightly increased. Meanwhile, the fluid shear stress increased with the lattice scaffold pore shape changing from 90° to 15°, the maximum fluid shear stress magnitude of scaffold 90° was 1.41 times higher than the one with 15°.

It is interesting that by the assembly of the scaffold with intersection angles from 90° to 15° within a single pore shape gradient scaffold structure could create a gradient increasing change of fluid velocity and fluid shear stress. This could be due to the dimension of scaffolds with pore shape from 90° to 15° specimen was the same. By changing the filament intersection angle from 90° to 15°, the pore numbers within scaffold are decreasing. Although those scaffolds had the same pore width as 0.6 mm and porosity as 52.4 %, the decreasing of pore number could cause slightly hinder the flow-through and create the slightly increase fluid velocity and shear stress from 90o scaffolds to 15° scaffolds.

The influence of layer configuration gradient

The layer configuration gradient that changing from lattice to stagger structures, their maximum fluid velocity magnitude was slightly increasing. In Fig. 5(d), the fluid velocity magnitude of the scaffold with lattice and stagger structure is 1.2 mm/s and 1.5 mm/s, respectively. This could be due to that the offset layer within the staggered structure spatially create a relative smaller 3D pore comparing the lattice structure and hindering the flow through.

Meanwhile, the fluid shear stress within stagger was higher than the lattice structure, which is a similar trend of their corresponding uniform structures. The maximum fluid shear stress magnitude of stagger scaffold was 1.89 times higher than the lattice. The lattice and stagger structures were assembly together as a layer configuration gradient

Table 3
A summary of parameters within the complex gradient structure from 1 to 10 zones.

	Filament diameter (mm)	Pore width (mm)	Layer configuration	Pore shape	Porosity
Zone 1	0.4	2.1	Lattice	90°	83.2 %
Zone 2	0.4	1.2	Lattice	90°	77.0 %
Zone 3	0.4	1.2	Stagger	90°	76.3 %
Zone 4	0.4	0.6	Lattice	90°	68.1 %
Zone 5	0.6	0.6	Lattice	90°	52.8 %
Zone 6	0.6	0.6	Lattice	75°	52.4 %
Zone 7	0.6	0.6	Lattice	60°	52.4 %
Zone 8	0.6	0.6	Lattice	45°	52.4 %
Zone 9	0.6	0.6	Lattice	30°	52.4 %
Zone 10	0.6	0.6	Lattice	15°	52.4 %

could also create a gradient change of fluid velocity and fluid shear stress.

Complex gradient structure

Based on those CFD simulation results from the uniform structures and single gradient structures, they demonstrate that the trend of fluid velocity and shear stress remains as the same as the criteria corresponding to every point compares to a particular uniform structure. The criteria were summarised as: (1) When keeping pore width (d_{xy}) as the same, the fluid velocity and shear stress within the lattice scaffold decrease with the filament diameter (d) decreasing; (2) When keeping filament diameter (d) as the same, the fluid velocity and shear stress within the scaffold increase with the pore width (d_{xy}) decreasing; (3) When keeping pore width (d_{xy}) and filament diameter (d) the same, the fluid velocity and shear stress within the scaffold increase with the
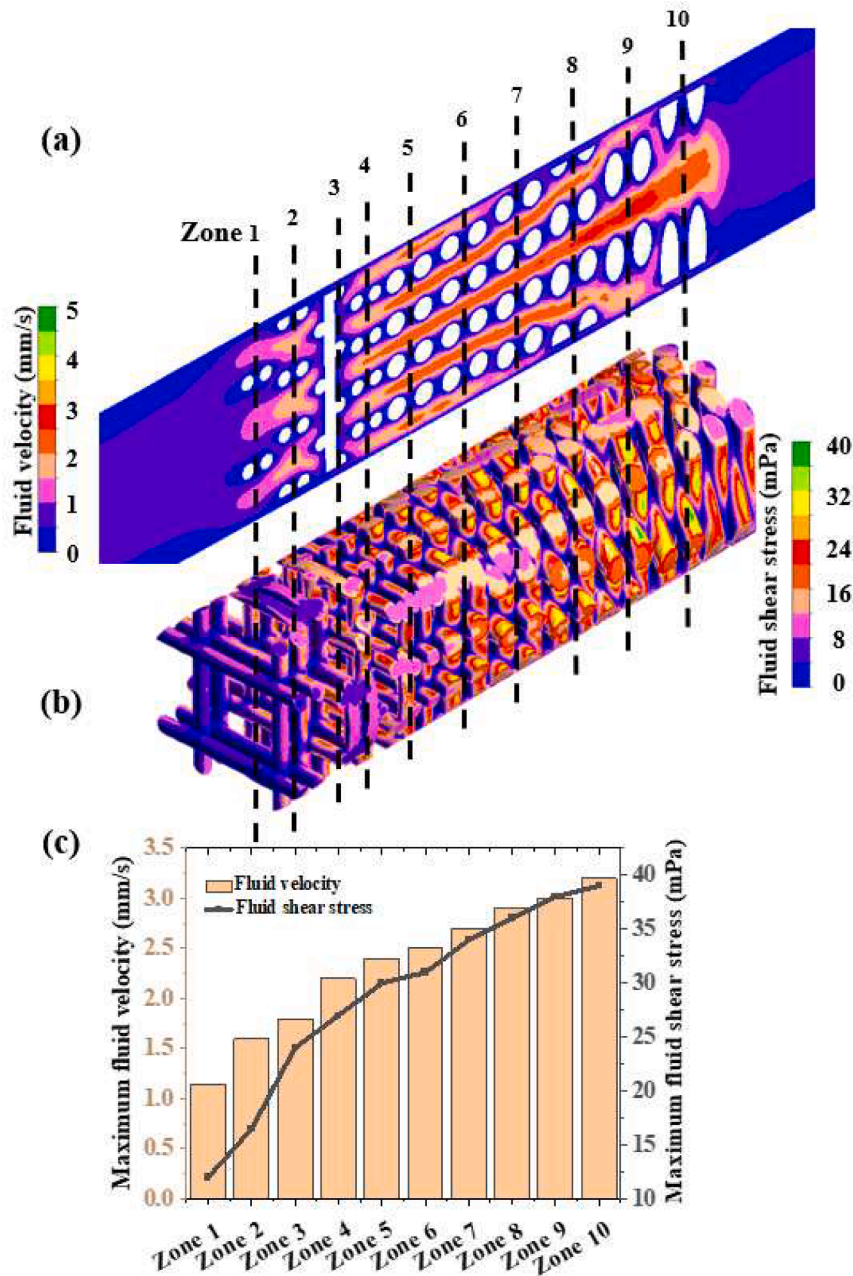
Fig. 6. Fluid velocity (a) and shear stress (b) within a complex gradient structure and their maximum magnitude of fluid velocity and wall shear stress within zone 1–10 (c).

filament intersection angle from 90° to 15°; (4) When keeping pore width (d_{xy}) and filament diameter (d) the same, the fluid velocity and shear stress within the staggered scaffold would larger than the lattice one.

Based on those criteria, this study proposes the idea that by assembly the variable geometries to create a complex gradient structure, its combination detail as Table 3. From Zone 1 to Zone 2 was the gradient change of pore width; from zone 2 to zone 3 was the gradient change from lattice to stagger structure; from zone 4 to zone 5 was the gradient change of filament diameter; from zone 5 to zone 10 was the gradient change of pore shape. The porosity had a gradient decrease within the complex gradient structure from Zone 1 to Zone 10, and the porosity was calculated based on the Eq (1) and 2.

Fig. 6 (a, b) shows the fluid velocity and shear stress distribution from Zone 1 to Zone 10 within the complex gradient structure with the combination of variable scaffold types. The black dash lines represent the middle plane of each type of scaffold structures, which is corresponding to each Zone. The maximum magnitude fluid velocity (from the longitudinal plane) and the maximum magnitude shear stress (from the transverse plane) were compared from each type of scaffolds.

The results show that the maximum magnitude of fluid velocity and fluid shear stress increased from Zone 1 to Zone 10. The pore width (d_{xy}) changed from 2.1 mm to 1.2 mm from Zone 1 to Zone 2, the fluid velocity and wall shear stress increase from 1.15 mm/s to 1.6 mm/s, and 12.0 to 16.5 mPa, respectively. Zone 2 to Zone 3 were the change from lattice structure to stagger structure, the fluid velocity and wall shear stress increase from 1.6 mm/s to 1.8 mm/s, and 16.5 to 24.0, respectively. The filament diameter (d) changed from Zone 4 to Zone 5, and their fluid velocity and wall shear stress increase from 2.2 to 2.4 mm/s, and 27 mPa to 30 mPa, respectively. Zone 5 to Zone 10 were the pore shape change that the filament intersection angle from 90° to 15°, the fluid velocity and wall shear stress increase from 2.4 mm/s to 3.2 mm/s, and 30 mPa to 39 mPa, respectively. The maximum fluid shear stress magnitude in Zone 1 scaffold was 3.25 times higher than the Zone 10.

It is interesting that the trend of the maximum magnitude of wall shear stress within the complex gradient structure remains as the same as the criteria corresponding to uniform structures. The gradient changing of fluid microenvironment could be controlled by the assembly of the scaffold with variable uniform geometries. Meanwhile, it is noted that uncoupled fluid-structure were assumed for the scaffold. This approximation does not consider the influence of scaffold deformation generated by the fluid flow, and the scaffold was assumed as rigid and impermeable. Since the maximum fluid shear stress on the scaffolds was less than 40 mPa, it is assumed that the filament deformation caused by solid-fluid interaction can be neglected.

Conclusions

This study systematically with CFD modelling to investigate the influence of scaffold filament diameter, pore width, pore shape and layer configuration on the magnitude and statistical distribution of fluid velocity and shear stress. A complex gradient scaffold structure was designed by assembling with the variable filament diameter, pore width, pore shape and layer configuration. The results show that the fluid distribution within the gradient structure was kept as the same as the corresponding their uniform structures. The fluid dynamic rules found in the uniform scaffold structures could be useful criteria for the designing of the gradient scaffold structure.

The CFD results show that the fluid velocity and shear stress within the newly designed complex gradient structure was created gradually increasing. Gradient fluid flow distribution was found within the scaffolds, suggesting that cells would be exposed to different stimulations, which could guide the development of scaffolds for multi-phase tissue. Meanwhile, CFD modelling allowed a detailed exploration of velocity maps inside the scaffolds, which could be beneficial to optimise the initial conditions of scaffold cell seeding under fluid flow.

Declaration of competing interest

There are no competing interests to declare.

Declarations

There are no conflicts to declare.

Ethical Approval

The research does not involve human subjects and ethical approval is not required.

References

[1] Zhang B, Nguyen AK, Narayan RJ, Huang J. "Direct ink writing of vancomycin-loaded polycaprolactone/polyethylene oxide/hydroxyapatite 3D scaffolds". Journal of the American Ceramic Society 2022;105(3):1821–40.

[2] Zhang B, Chung SH, Barker S, Craig D, Narayan RJ, Huang J. "Direct ink writing of polycaprolactone/polyethylene oxide based 3D constructs". Progress in Natural Science: Materials International 2021;31(2):180–91.

[3] Zhang B, Huang J, Narayan RJ. "Gradient scaffolds for osteochondral tissue engineering and regeneration". Journal of Materials Chemistry B 2020;8(36): 8149–70.

[4] Seidi A, Ramalingam M, Elloumi-Hannachi I, Ostrovidov S, Khademhosseini A. "Gradient biomaterials for soft-to-hard interface tissue engineering". Acta Biomater 2011;7(4):1441–51.

[5] Rao RT, Browe DP, Lowe CJ, Freeman JW. "An overview of recent patents on musculoskeletal interface tissue engineering". Connect Tissue Res 2016;57(1): 53–67.

[6] Bayrak E, Yilgor Huri P. "Engineering musculoskeletal tissue interfaces". Front Mater 2018;5:24.

[7] Dormer NH, Singh M, Wang L, Berkland CJ, Detamore MS. "Osteochondral interface tissue engineering using macroscopic gradients of bioactive signals". Ann Biomed Eng 2010;38(6):2167–82.

[8] Carrubba VLa, Pavia FC, De Luca A, Giavaresi G. "Composite Scaffolds with a Hydrohyapatite Spatial Gradient for Osteochondral Defect Repair". 2018 IEEE 4th international forum on research and technology for society and industry (RTSI). IEEE; 2018. p. 1–4.

[9] Parisi C, et al. "Biomimetic gradient scaffold of collagen–hydroxyapatite for osteochondral regeneration". J Tissue Eng 2020;11:2041731419896068.

[10] Liu W, et al. "Rapid continuous multimaterial extrusion bioprinting". Advanced materials 2017;29(3):1604630.

[11] Loh QL, Choong C. Three-dimensional scaffolds for tissue engineering applications: role of porosity and pore size. Tissue Engineering Part B: Reviews 2013;19(6): 485–502.

[12] Meyer U, Büchter A, Nazer N, Wiesmann H. "Design and performance of a bioreactor system for mechanically promoted three-dimensional tissue engineering". British Journal of Oral and Maxillofacial Surgery 2006;44(2):134–40.

[13] Kim KM, et al. "Shear stress induced by an interstitial level of slow flow increases the osteogenic differentiation of mesenchymal stem cells through TAZ activation". PLoS One 2014;9(3):e92427.

[14] Lee DA, Knight MM, Campbell JJ, Bader DL. "Stem cell mechanobiology". J Cell Biochem 2011;112(1):1–9.

[15] Kim DH, Heo SJ, Kim SH, Shin JW, Park SH, Shin JW. "Shear stress magnitude is critical in regulating the differentiation of mesenchymal stem cells even with endothelial growth medium". Biotechnol Lett 2011;33(12):2351–9.

[16] Kreke MR, Huckle WR, Goldstein AS. "Fluid flow stimulates expression of osteopontin and bone sialoprotein by bone marrow stromal cells in a temporally dependent manner". Bone 2005;36(6):1047–55.

[17] Xu H, et al. "Impact of flow shear stress on morphology of osteoblast-like IDG-SW3 cells". J Bone Miner Metab 2018;36(5):529–36.

[18] Hislop BD, Heveran CM, June RK. "Development and analytical validation of a finite element model of fluid transport through osteochondral tissue". bioRxiv 2020.

[19] Zhang B, Belton P, Teoh XY, Gleadall A, Bibb R, Qi S. "An investigation into the effects of ink formulations of semi-solid extrusion 3D printing on the performance of printed solid dosage forms". Journal of Materials Chemistry B 2024;12(1): 131–44.

[20] Zhang B, et al. "Development of combi-pills using the coupling of semi-solid syringe extrusion 3D printing with fused deposition modelling". Int J Pharm 2022;625: 122140.

[21] Zhang B, Gleadall A, Belton P, Mcdonagh T, Bibb R, Qi S. "New insights into the effects of porosity, pore length, pore shape and pore alignment on drug release from extrusionbased additive manufactured pharmaceuticals". Addit Manuf 2021; 46:102196.

[22] Qi S, Zhang B, McDonagh T. "Three-dimensional Printed Implantable Products". in Implantable Technologies 2021:252–95.

[23] Boschetti F, Raimondi MT, Migliavacca F, Dubini G. "Prediction of the micro-fluid dynamic environment imposed to three-dimensional engineered cell systems in bioreactors". J Biomech 2006;39(3):418–25.

[24] Melchels FP, et al. "The influence of the scaffold design on the distribution of adhering cells after perfusion cell seeding". Biomaterials 2011;32(11):2878–84.

[25] Omar AM, et al. "Geometry-based computational fluid dynamic model for predicting the biological behavior of bone tissue engineering scaffolds". J Funct Biomater 2022;13(3):104.

[26] Youssef K, Mack J, Iruela-Arispe M, Bouchard LS. "Macro-scale topology optimization for controlling internal shear stress in a porous scaffold bioreactor". Biotechnol Bioeng 2012;109(7):1844–54.

[27] Watson E, Mikos AG. "Advances in In Vitro and In Vivo Bioreactor-Based Bone Generation for Craniofacial Tissue Engineering". BME Front 2023;4:0004.

[28] Liu Z, et al. "Cell seeding process experiment and simulation on three-dimensional polyhedron and cross-link design scaffolds". Front Bioeng Biotechnol 2020;8:104.

[29] VandenHeuvel DJ, Devlin BL, Buenzli PR, Woodruff MA, Simpson MJ. "New computational tools and experiments reveal how geometry affects tissue growth in 3D printed scaffolds". Chemical Engineering Journal 2023;475:145776.

[30] Choe R, et al. "Computational investigation of interface printing patterns within 3D printed multilayered scaffolds for osteochondral tissue engineering". Biofabrication 2022;14(2):025015.

[31] Fallah A, et al. "3D printed scaffold design for bone defects with improved mechanical and biological properties". J Mech Behav Biomed Mater 2022;134: 105418.

[32] Liu H, Ahlinder A, Yassin MA, Finne-Wistrand A, Gasser TC. "Computational and experimental characterization of 3D-printed PCL structures toward the design of soft biological tissue scaffolds". Mater Des 2020;188:108488.

[33] Zhang B. "Computational fluid dynamics analysis of the fluid environment of 3D printed tissue scaffolds within a perfusion bioreactor: the effect of pore shape". Procedia Structural Integrity 2023;49:3–9.

[34] Bittner SM, et al. "Fabrication and mechanical characterization of 3D printed vertical uniform and gradient scaffolds for bone and osteochondral tissue engineering". Acta Biomater 2019;90:37–48.

[35] Andrea Di Luca B, Lorenzo-Moldero Ivan, Lepedda Antonio, Swieszkowski Wojcech, Blitterswijk ClemensVan, Moroni Lorenzo. "Gradients in pore size enhance the osteogenic differentiation of human mesenchymal stromal cells in three-dimensional scaffolds". Sci Rep 2015. https://doi.org/10.1038/ srep22898.

[36] Gao F, et al. "Direct 3D printing of high strength biohybrid gradient hydrogel scaffolds for efficient repair of osteochondral defect". Adv Funct Mater 2018;28 (13):1706644.

[37] Weinbaum S, Cowin S, Zeng Y. "A model for the excitation of osteocytes by mechanical loading-induced bone fluid shear stresses". J Biomech 1994;27(3): 339–60.

[38] Yan X, Chen X, Bergstrom D. "Modeling of the flow within scaffolds in perfusion bioreactors". Am J Biomed Eng 2011;1(2):72–7.

[39] Jungreuthmayer C, et al. "The 3D pore structure and fluid dynamics simulation of macroporous monoliths: High permeability due to alternating channel width". Journal of Chromatography A 2015;1425:141–9.

[40] Nokhbatolfoghahaei H, et al. "Computational modeling of media flow through perfusion-based bioreactors for bone tissue engineering". Proceedings of the Institution of Mechanical Engineers 2020;234(12):1397–408. Part H: Journal of Engineering in Medicine.